



# Study on the surface properties of colored talc filler (CTF) and mechanical performance of CTF/acrylonitrile-butadiene-styrene composite

Zhitong Yao <sup>a</sup>, Jerry Y.Y. Heng <sup>b</sup>, Senentxu Lanceros-Méndez <sup>c</sup>, Alessandro Pegoretti <sup>d</sup>, Xiaosheng Ji <sup>e,\*</sup>, Eftychios Hadjitosifis <sup>b</sup>, Meisheng Xia <sup>e</sup>, Weihong Wu <sup>a</sup>, Junhong Tang <sup>a,\*\*</sup>

<sup>a</sup> College of Materials Science and Environmental Engineering, Hangzhou Dianzi University, Hangzhou, 310018, China

<sup>b</sup> Department of Chemical Engineering, Imperial College London, South Kensington Campus, London, SW7 2AZ, United Kingdom

<sup>c</sup> Centro/Departamento de Física, Universidade do Minho, 4710-057, Braga, Portugal

<sup>d</sup> Department of Industrial Engineering and INSTM Research Unit, University of Trento, Via Sommarive 9, 38123, Trento, Italy

<sup>e</sup> Ocean College, Zhejiang University, Zhoushan, 316021, China



## ARTICLE INFO

### Article history:

Received 16 December 2015

Received in revised form

13 March 2016

Accepted 23 March 2016

Available online 25 March 2016

### Keywords:

Talc

Filler

Inverse gas chromatography

Contact angle

Acrylonitrile-butadiene-styrene

## ABSTRACT

In this work, a novel colored talc filler (CTF) was prepared, and its surface properties were subsequently studied and compared to those of talc filler (TF) using inverse gas chromatography (IGC) and contact angle measurement. The mechanical properties of acrylonitrile-butadiene-styrene (ABS) composites filled with CTF and TF were investigated as well. The results indicated that the dispersive component ( $\gamma_S^D$ ) for both samples contributed the major part of the total surface energy ( $\gamma_S^T$ ). The values determined by the contact angle methods were consistent, although lower than those using IGC analysis. Compared to  $\gamma_S^D$ , the polar component ( $\gamma_S^{SP}$ ) contributed less to  $\gamma_S^T$ , implying a lower polarity for both samples. The  $\gamma_S^{SP}$  values calculated by the contact angle methods were also consistent and lower than those calculated using IGC. The lower  $\gamma_S^T$  value for CTF could reduce filler particle-particle interactions, allowing a better dispersion in ABS matrix, and thus leading to an increase in ABS/CTF composite performance.

© 2016 Elsevier B.V. All rights reserved.

## 1. Introduction

Talc is a plate-like layered structure magnesium silicate mineral, in which the octahedral brucite layer is sandwiched between two tetrahedral silica sheets. Many reports have indicated an improvement in performance after a polymer matrix was reinforced with talc filler [1–5]. However, it has been widely recognized that the filler nature of talc influences its reinforcement ability, depending on the surface activity, particle size, surface area, and surface functional groups [6,7]. Among these properties, surface activity affects the reinforcement ability of filler the most, because the chemical nature of a particle's surface determines filler–filler and filler–matrix interactions. These interactions in turn affect the filler's dispersion in the polymer matrix and thus the final

performance of the composite. Therefore, a better understanding of a filler's surface properties is critical for determining the most effective polymer reinforcement fillers.

However, to the best of our knowledge, the surface characterization of talc-derived fillers has been poorly reported and is poorly understood. In this work, a colored talc filler (CTF) was prepared, and its surface properties were subsequently studied and compared to those of talc filler (TF), using IGC and contact angle measurement. The mechanical properties of ABS composites filled with CTF and TF were investigated as well.

## 2. Basic theory

### 2.1. IGC method

#### 2.1.1. Surface energy

In IGC, the solids to be characterized are packed into columns, and different gases are injected. The injection of known polar and nonpolar gases enables the determination of the surface properties of the packed materials. Molecular probes are injected at infinite

\* Corresponding author.

\*\* Corresponding author.

E-mail addresses: [jixiaoshen@hotmail.com](mailto:jixiaoshen@hotmail.com), [sxyzt@126.com](mailto:sxyzt@126.com) (X. Ji), [tang\\_jhjh@163.com](mailto:tang_jhjh@163.com) (J. Tang).

dilution to rule out lateral probe-probe interactions and to favor probe-stationary phase interactions only. Stationary phase characterization is achieved by partitioning the samples between the mobile and stationary phases.

According to Fowkes [8–10], the total surface energy ( $\gamma_S^T$ ) is often divided into dispersive ( $\gamma_S^D$ ) and specific ( $\gamma_S^{SP}$ ) surface energy components. The dispersive interactions consist of London, Keesom and Debye interactions, while the specific interactions include acid-base interactions, H-bonding and  $\pi$ -bonding.

$$\gamma_S^T = \gamma_S^D + \gamma_S^{SP} \quad (1)$$

A standard procedure of solid surface characterization is that the  $\gamma_S^D$  is first calculated using a series of *n*-alkanes as probes (in this case, Hexane, Heptane, Octane, Nonane and Decane); then the acid-base parameters can be determined from the dispersive parameters with acid-base probe molecules (in this case, Dichloromethane (DCM), Toluene, Chloroform). For the calculation of  $\gamma_S^D$ , the Dorris-Gray method [11] is commonly used and thus it was applied in this work. The contribution of acid-base properties is often obtained by first measuring the specific Gibbs free energies of adsorption ( $\Delta G^{SP}$ ) for the various polar probes. From the  $\Delta G^{SP}$ , it can be calculated the acid-base numbers related to the specific surface energy. Based on the van-Oss-Chaudhury-Good (vOCG) approach [12] and applying the Della Volpe scale [13] for surface tension components of polar solvents, the  $\gamma_S^{SP}$  is subdivided into Lewis acid ( $\gamma_S^+$ ) and Lewis base ( $\gamma_S^-$ ) components.

$$\gamma_S^{SP} = 2\sqrt{\gamma_S^+ \gamma_S^-} \quad (2)$$

### 2.1.2. Deconvolution of surface energetic sites

Surface energy heterogeneity, manifesting with a distribution of various surface sites with different energy levels, constitutes an energetic map of the solid surface and thus allows a prediction of the materials properties, in particular the formulation of composites, adhesives or blends. Such a heterogeneity profile can be represented by an energy distribution function. IGC is not the only means of measuring surface energy heterogeneity and alternative techniques are considered for measuring surface free energy. However, the contact angle measurement requires macroscopic crystals in order to determine specific energy contributions. Such measurements on specific crystalline facets may neglect edge effects and defects, and reflect a bulk average surface energy for solids. Another approach is adhesion force measurement by atomic force microscopy, although there are theoretical and technical challenges to this methodology. IGC provides data over a wide range of probe surface coverages, yielding information about the relative heterogeneity of the surface energy distribution of a material. However, existing methods for interpreting IGC data are based on inappropriate assumptions, giving purview to the development of new approaches to the analysis of surface-energy heterogeneity.

A more robust method for computing the surface energy distribution of heterogeneous powders has recently been proposed. Based on sounder thermodynamic assumptions, Smith et al. [14] developed a new numerical model for energy calculation, expanding on initial efforts from the model proposed by Jefferson et al. [15]. Using this approach, the surface energy distribution is determined by fitting simulation parameters to experimental IGC data. A computer algorithm is used that varies the model parameters and compares the resulting simulation with the experimental data. The process is repeated until small changes in the model parameters do not improve the fit of the simulation to the

experimental data. It is worth noting that, the use of thermodynamic principles for the filling of energetic sites is an important step in characterizing the effect of differing energetic contributions. This is a nontrivial problem, as can be seen by the nonlinear relationship displayed by mixtures of materials at different energies. In this instance, it would seem appropriate to use multiple single energy values at different weights, to simulate the different states. To account for slight defects around these energy sites, the use of Gaussian distribution for each was used:

$$f(\gamma_S^D) = \frac{1}{\sigma\sqrt{2\pi}} \exp\left[-\frac{1}{2}\left(\frac{\gamma_S^D - \mu}{\sigma}\right)^2\right] \quad (3a)$$

where  $\sigma$  represents the standard deviation and  $\mu$  is the center of the energy. The standard deviations of the Gaussian functions are fixed at one. The distributions for all the energy states are then combined to form a single distribution, whose sum is normalized to the value 1 (as this sets the total energy sites to 100% of the surface).

### 2.2. Contact angle methods

There are numerous methods for calculating the solid surface energy from equilibrium liquid contact angles. Among these methods, the Zisman plot [16–18], Fowkes [19,20], Owens-Wendt-Kaelble (OWK) [21,22], vOCG [23] and Wu [24,25] are commonly used and thus were applied in this work.

The key equation used to determine the solid surface energies by contact angle measurement is the Young's equation [26], which was derived from the equilibrium condition of forces representing surface tensions at the contact point of three phases: solid, liquid and gas.

$$\gamma_L \cos \theta = \gamma_S - \gamma_{SL} \quad (3b)$$

where  $\gamma_S$ ,  $\gamma_L$  and  $\gamma_{SL}$  are the surface free energies of solid, liquid and solid–liquid ( $\text{mJ/m}^2$ ), respectively; and  $\theta$  is the contact angle between the solid surface and the test liquid ( $^\circ$ ).

In the Young's equation, both  $\theta$  and  $\gamma_L$  are measurable. In order to obtain  $\gamma_S$  and  $\gamma_{SL}$  by solving this equation, an additional relationship between these quantities has to be made. An understanding of the different methods requires an explanation of the term "work of adhesion ( $W_A$ )". Thermodynamic adhesion is the *de facto* energy spent to restructure the bonded interface due to the atomistic interaction between two materials. The equation for  $W_A$  can be written as:

$$W_A = \gamma_A + \gamma_B - \gamma_{AB} \quad (4)$$

where  $\gamma_A$  and  $\gamma_B$  represent the surface tensions of phases A and B; and  $\gamma_{AB}$  represents the interfacial tension between the two phases. For the solid–liquid system, the equation can be written as:

$$W_A = \gamma_S + \gamma_L - \gamma_{SL} \quad (5)$$

Combining it with the Young's equation yields:

$$W_A = \gamma_L(1 + \cos \theta) \quad (6)$$

In a similar way, the work of cohesion ( $W_C$ ) of one substance (e.g., A) can be defined as:

$$W_C = \gamma_A + \gamma_A - 0 = 2\gamma_A \quad (7)$$

Berthelot [27] stabilized the direction to surface energy calculations and assumed that  $W_A$  between the solid and the liquid equals the geometric mean of individual cohesion work.

$$W_A = \sqrt{W_{SS}W_{LL}} \quad (8)$$

Combining Eq. (8) with Eqs. (6) and (7) yields:

$$W_A = \sqrt{W_{SS}W_{LL}} = 2\sqrt{\gamma_S\gamma_L} = \gamma_L(1 + \cos\theta) \quad (9)$$

### 2.2.1. Zisman plot method

The interpretation of contact angles in terms of solid surface energy was pioneered by Zisman and Fox [16–18]. A Zisman plot is used to define the so-called critical surface tension ( $\gamma_c$ ) of wetting, which differs from the surface energy and is not divided into dispersive and nondispersive (polar) components. The key observation they made was that, for a given solid, the measured contact angles did not vary randomly as the liquid varied; rather, the  $\cos\theta$  changed smoothly with the  $\gamma_L$ , suggesting a straight-line relationship. The linear-regression extrapolated value of  $\gamma_L$  at  $\cos\theta = 1$  equals  $\gamma_c$ . In this theory, only two measurement points would be needed; thus, the  $\gamma_c$  values for TF and CTF were determined using water and formamide as the test liquids in this work.

### 2.2.2. Fowkes method

According to Fowkes [19,20], the dispersive interactions between nonpolar solid and liquid are predominant and connected with London forces. Thus, he used only the dispersive component in the equation for solid–liquid interfacial forces.

$$\gamma_{SL} = \gamma_S + \gamma_L - 2\sqrt{\gamma_S^D\gamma_L^D} \quad (10)$$

Combining Eq. (10) with the Young's equation yields:

$$\gamma_L(1 + \cos\theta) = 2\sqrt{\gamma_S^D\gamma_L^D} \quad (11)$$

For this method, only the dispersive component of the interface interactions is specified. Thus, it is more suited for determining the dispersive contribution to the total surface energy. Since there is one unknown,  $\gamma_S^D$ , in this equation, one liquid with known dispersive component can be used to solve it. In this work, the  $\gamma_S^D$  values for TF and CTF were determined using diiodomethane as the test liquid.

### 2.2.3. OWK method

Owen and Wendt extended Fowkes' idea and added the polar component of surface energy to the solid–liquid interfacial forces. This consists in determining the dispersive and polar components of surface energy based on Berthelot's principle [27]. Owens and Wendt proposed the following form for  $W_A$ :

$$W_A = 2\sqrt{\gamma_S^D\gamma_L^D} + 2\sqrt{\gamma_S^{SP}\gamma_L^{SP}} \quad (12)$$

Combining it with the Young's equation leads to Eq. (13):

$$\gamma_L(1 + \cos\theta) = 2\sqrt{\gamma_S^D\gamma_L^D} + 2\sqrt{\gamma_S^{SP}\gamma_L^{SP}} \quad (13)$$

Since there are two unknowns,  $\gamma_S^D$  and  $\gamma_S^{SP}$ , in this equation, at least two liquids with known dispersive and polar components are needed to solve it. The liquid with the dominant polar component should be chosen as one test liquid and the dispersive liquid as the other. Distilled water, glycerol and formamide can be used as polar liquids, diiodomethane and  $\alpha$ -bromonaphthalene as dispersive. In this work, the surface energy parameters for TF and CTF were determined using formamide and diiodomethane as the test liquids.

### 2.2.4. vOCG method

Van Oss et al. [28–30] followed Fowkes' theory and treated surface energy as a sum of the apolar Lifshitz-van der Waals component ( $\gamma_S^{LW}$ , similar to  $\gamma_S^D$ ) and a polar component ( $\gamma_S^{AB}$ , similar to  $\gamma_S^{SP}$ ). The interfacial tension was postulated for solid–liquid systems as:

$$\gamma_{SL} = \gamma_S + \gamma_L - 2\left[\sqrt{\gamma_S^{LW}\gamma_L^{LW}} + \sqrt{\gamma_S^+\gamma_L^-} + \sqrt{\gamma_S^-\gamma_L^+}\right] \quad (14)$$

Combining it with the Young's equation, we can obtain:

$$\gamma_L(1 + \cos\theta) = 2\sqrt{\gamma_S^{LW}\gamma_L^{LW}} + 2\sqrt{\gamma_S^+\gamma_L^-} + 2\sqrt{\gamma_S^-\gamma_L^+} \quad (15)$$

Since there are three unknowns,  $\gamma_S^{LW}$ ,  $\gamma_S^+$  and  $\gamma_S^-$ , in this equation, at least three test liquids with known surface energy components are needed to solve it. One dispersive (e.g. diiodomethane) and two polar (e.g. water, glycerol) liquids could be used. In this work, distilled water, formamide and diiodomethane were applied.

### 2.2.5. Wu method

In addition to the OWK method, the other two-liquid method for considering the harmonic mean relationship was proposed by Wu [24,25]. He discerns between dispersive and polar components of the surface energy, but instead of using the geometric mean as in Eq. (13), he uses a harmonic mean in the expression for  $\gamma_{SL}$ .

$$\gamma_{SL} = \gamma_S + \gamma_L - 4\left[\frac{\gamma_S^D\gamma_L^D}{\gamma_S^D + \gamma_L^D} + \frac{\gamma_S^{SP}\gamma_L^{SP}}{\gamma_S^{SP} + \gamma_L^{SP}}\right] \quad (16)$$

In combination with the Young's equation, Wu's equation can be written as:

$$\gamma_L(1 + \cos\theta) = \frac{4\gamma_S^D\gamma_L^D}{\gamma_S^D + \gamma_L^D} + \frac{4\gamma_S^{SP}\gamma_L^{SP}}{\gamma_S^{SP} + \gamma_L^{SP}} \quad (17)$$

As in the OWK method, Wu's method also requires the use of at least two liquids. In this work, the surface energy parameters for TF and CTF were calculated using formamide and diiodomethane as the test liquids.

## 3. Experimental section

### 3.1. Materials

ABS copolymer (XR 401), composed of 24 wt% acrylonitrile, 6 wt% butadiene, and 70 wt% styrene, was supplied by LG Chemical Ltd. Direct Red 28 (DR 28) was provided by Yiwu Yu Fang Pigment Co., Ltd., China. Raw black talc was purchased from Guang Feng Tian Tu Chemical Co., Ltd., China. It was calcined at high temperature to remove the impurities and obtain the talc filler (TF).

### 3.2. CTF preparation

The TF powders were mixed with DR 28, water and hexadecyltrimethylammonium bromide at a weight ratio of 20: 2: 8.5: 1. After vigorous stirring, the mixture was left standing for 24 h. Then it was filtered and the filter cake was dried. The dried cake was ground to obtain the colored talc filler (CTF). Photographs of the TF and CTF powders are displayed in Fig. 1.

### 3.3. ABS composites preparation

Before mixing, the talc fillers and ABS matrix were oven-dried. Various weight ratios of ABS and talc fillers (100/0, 98/2, 95/5, 90/

10, 85/15, 80/20, 70/30 and 60/40) were mixed with 0.1 wt% antioxidant, 1.0 wt% lubricant and 0.1 wt% mineral oil, using a SHJ-35 parallel co-rotating twin screw extruder (Nanjing, China). The extrudates were pelletized, and then a plastic injection molding machine (MA900/260, Ningbo, China) was used to prepare the test specimens. Prior to testing, impact and tensile dumb-bell bars were conditioned at a temperature of  $23 \pm 2$  °C and relative humidity of  $50 \pm 5\%$  for 40 h.

### 3.4. Characterization and tests

The surface-energy characterization of talc fillers was carried out using an iGC Surface Energy Analyzer (iGC-SEA, Surface Measurement Systems, Alperton, UK). Approximately 300 mg of the powders were packed into individual dimethyldichlorosilane-treated glass columns. The samples were run at surface coverages of 0.005–0.1% with polar and nonpolar molecular probes, to determine the  $\gamma_s^D$  and  $\gamma_s^{SP}$  as well as the  $\Delta G^{SP}$ . The sample column was preconditioned for 1 h at 343.15 K and 0% RH with 10 ml/min helium carrier gas, under the same conditions as in the experiment. The contact angles of TF and CTF for test liquids (distilled water, formamide and diiodomethane) were measured using the sessile drop method. The surface tension and its components for the test liquids are listed in Table 1. The contact angle measurement was carried out at 20 °C and the ambient humidity using a goniometer (DSA100, Krüss GmbH, Germany). The uniaxial tensile tests of ABS composites were conducted according to the ASTM D638 standard. The Izod impact test was carried out on unnotched specimens according to the ASTM D256 standard.

## 4. Results and discussion

### 4.1. IGC method

The  $\gamma_s^D$ ,  $\gamma_s^{SP}$  and  $\gamma_s^T$  profiles for the TF and CTF obtained from iGC-SEA are displayed in Fig. 2. It can be observed that the  $\gamma_s^D$  component for both samples contributed the major part (72–81%) of  $\gamma_s^T$ . In addition, the surface energy displayed a decreasing trend with increasing surface coverage and the highest energy sites occupied approximately 0.5% of the fillers. The difference in the measured absolute  $\gamma_s^D$  values at low and high coverages indicated heterogeneity among surface energy sites. For TF, the calculated  $\gamma_s^D$  fell into the range of 121.6–170.6 mJ/m<sup>2</sup> across the surface coverages measured. As a comparison, the CTF showed a lower range of 51.1–76.8 mJ/m<sup>2</sup>. This was not completely consistent with the literature. Comard et al. [31] revealed that the surface properties of talc were influenced by particle size and grinding process rather than the geological origin. The carbonate content had no real

**Table 1**  
Surface tension and its components for the probe liquids.

Surface energy parameters (mJ/m <sup>2</sup> )	Water	Formamide	Diiodomethane
$\gamma_L$	72.8	58.0	50.8
$\gamma_L^D$	21.8	39.0	50.8
$\gamma_L^{SP}$	51.0	19.0	0
$\gamma^+$	25.5	2.28	0
$\gamma^-$	25.5	39.6	0

influence on these properties. They also studied the changes of  $\gamma_s^D$  as a function of polymer impregnation ratio for talc, and reported a high value of 160 mJ/m<sup>2</sup> for neat talc [32]. Douillard et al. [33] also revealed a value of 131 mJ/m<sup>2</sup>. However, Kaggwa et al. [34] and Giese et al. [35] reported lower values of 49 and 32 mJ/m<sup>2</sup> for talc, respectively. In this work, a decrement of  $\gamma_s^D$  for CTF was observed, which might be ascribed to its more uniform surface after loading with DR 28.

Compared to  $\gamma_s^D$ , the  $\gamma_s^{SP}$  component contributed less to  $\gamma_s^T$ : approximately 19% for TF and 28% for CTF, implying a lower polarity for both samples. The calculated  $\gamma_s^{SP}$  fell into the range of 28.8–40.0 mJ/m<sup>2</sup> for TF and 14.5–34.6 mJ/m<sup>2</sup> for CTF. According to literature, the  $\gamma_s^{SP}$  values for talc generally differed from these results. Wu et al. [36] studied the effect of grinding on the surface properties of talc and reported  $\gamma_s^{SP}$  values of 1.7 mJ/m<sup>2</sup> for talc and 4.2 mJ/m<sup>2</sup> for ground talc. Giese et al. [35] revealed a value of 5.1 mJ/m<sup>2</sup> for talc. The acid  $\gamma_s^+$  and basic  $\gamma_s^-$  components of the polar surface energy are also included in Fig. 2. It can be observed that the  $\gamma_s^+$  component was larger than the  $\gamma_s^-$ . This was not consistent with reports in the literature, where Wu et al. [36] revealed a  $\gamma_s^-$  value of 6.9 mJ/m<sup>2</sup> and a  $\gamma_s^+$  value of 0.1 mJ/m<sup>2</sup>. Giese et al. [35] also reported a higher value for  $\gamma_s^-$  (2.7 mJ/m<sup>2</sup>) than for  $\gamma_s^+$  (2.4 mJ/m<sup>2</sup>).  $\gamma_s^T$  is assumed to be the sum of  $\gamma_s^D$  and  $\gamma_s^{SP}$ , so that the higher  $\gamma_s^D$  and  $\gamma_s^{SP}$  for TF added up to a higher  $\gamma_s^T$  value.

Fig. 2 shows the surface energy profiles measured by IGC for TF and CTF. This surface energy profile was then analyzed using the approach delineated in section 2.1.2 to provide an array of energies for the materials surface. The deconvoluted surface energy is shown in Fig. 3. The energy values for CTF found by the computational method of 35, 80, and 140 mJ/m<sup>2</sup>, and similarly the energy values found computationally for TF were 120, 140, and 290 mJ/m<sup>2</sup>. As expected, all energetically heterogeneous samples had variations of surface sites.

### 4.2. Contact angle methods

The contact angles for TF and CTF determined using the sessile drop method are listed in Table 2. It can be observed that there was



**Fig. 1.** Photographs of the TF and CTF powders.

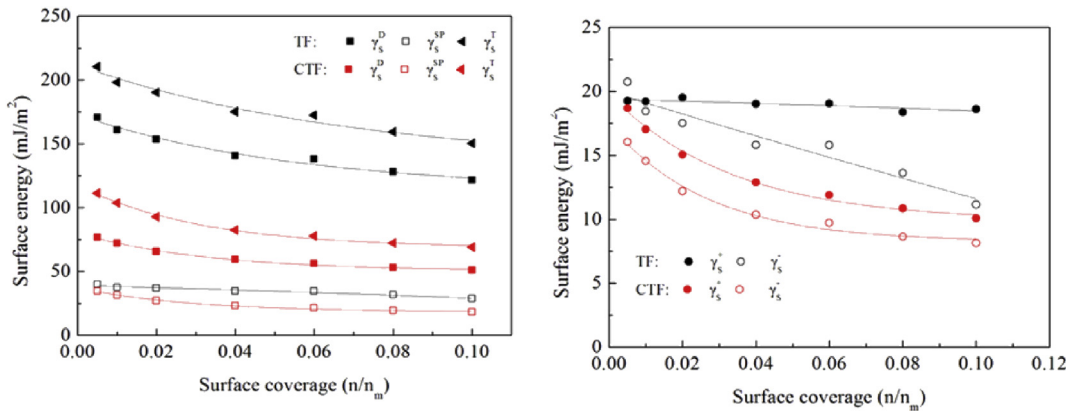


Fig. 2. Surface energy profiles for TF and CTF.

no distinction between the contact angles of the two samples. In addition, contact angles for the three liquids were all less than 90°, indicating an amphiphilic character for both samples. This was consistent with the results in the literature, where the contact angles of talc for water, formamide and diiodomethane were reported as 79, 43 and 42°, respectively [36]. Douillard et al. [37] revealed advancing contact angles of 60, 42 and 38° for water, formamide and diiodomethane, respectively.

#### 4.3. Surface energy comparsion

The surface energy profiles for TF and CTF determined using alkanes by IGC are displayed in Fig. 2. As a comparsion, the surface energy calculated using five contact angle methods are included in Table 2. It can be observed that the  $\gamma_S^D$  determined by the Fowkes, OWK, vOCG and Wu methods were consistent, but lower than those using IGC analysis. From a theoretical point of view, the results obtained from IGC and contact angle measurement are somewhat different. Ticehurst et al. [38] claimed that the  $\gamma_S^D$  results from the two methods cannot be identical because of the distinction in their theoretical approaches. In the surface characterization of phenol-formaldehyde-lignin resin, Matsushita et al. [39] and Dove et al. [40] also observed a discrepancy between the absolute values of  $\gamma_S^W$  calculated by the two methods. However, in the measurement of pharmaceutical powders, Planinšek et al. [41] found a good correlation between results obtained from the two methods. Thus, a satisfactory solution to this question would require further systematic study comparing data obtained from both methods. In fact, IGC analysis performed to determine  $\gamma_S^D$  is

mostly carried out under infinitely dilute conditions, where minimal doses of molecular probes are used. Therefore, any information obtained from IGC under these conditions will mainly concern the most active sites of the solid surfaces, which may constitute only a small fraction (e.g. 0.1%) of the surface examined. In addition, IGC evaluates mainly high energy sites, which is associated with preferential interactions of injected probes with these sites on the heterogeneous surface of stationary phase [42–44]. This in turn indicated the significance of surface energy distribution and thus the deconvolution of surface energetic sites was conducted in this work.

As for  $\gamma_S^{SP}$ , it fell into the range of 28.8–40.0 mJ/m<sup>2</sup> for TF and 14.5–34.6 mJ/m<sup>2</sup> for CTF, as determined by IGC. As a comparison, the  $\gamma_S^{SP}$  values calculated by the contact angle methods were less than those determined by the IGC method. A difference in  $\gamma_S^{SP}$  between the two methods was also reported [45], a result that can be expected because an infinite IGC operates at zero surface coverage of the probe molecules, and predominantly detects high energy sites [46]. Thus, the  $\gamma_S^{SP}$  values obtained by IGC will often be higher than those obtained by contact angle methods, as the latter detect surface sites of all energy levels (e.g. 100% of the surface sites) and thus determine an average energy level for the solid surface [47].

The  $\gamma_S^T$  values determined by IGC were in the range of 150.4–210.6 mJ/m<sup>2</sup> for TF and 56.9–111.4 mJ/m<sup>2</sup> for CTF. The values determined by OWK, vOCG and Wu methods were consistent, but less than those determined by IGC. According to Eq. (7),  $W_C$  equals  $2\gamma_S^T$ . Therefore, the CTF showed lower  $W_C$  as compared to TF, which could reduce the filler particle-particle interactions, allowing its better dispersion in a polymer matrix.

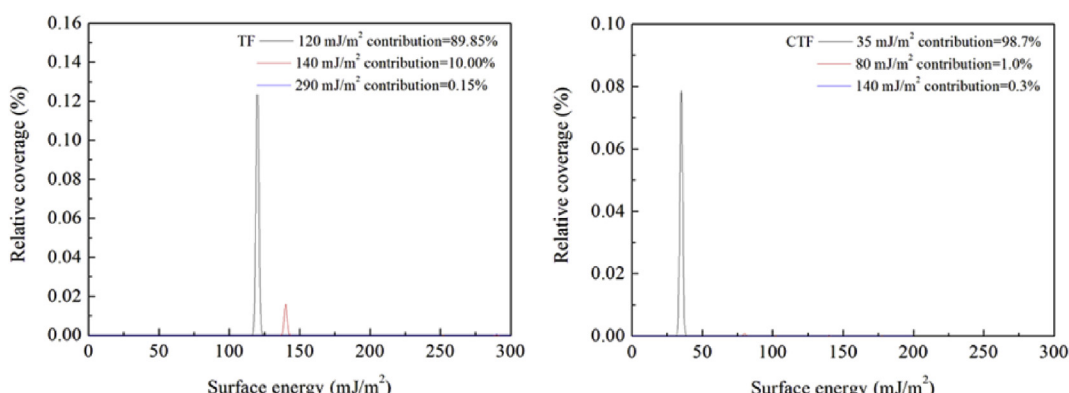


Fig. 3. Dispersive surface energy site distribution for TF and CTF.

**Table 2**

Surface energy and its components for two samples obtained by contact angle measurement ( $n = 5$ ).

Samples	Contact angles ( $^{\circ}$ ) $\pm$ SDn-1			Surface energy parameters (mJ/m <sup>2</sup> )															
				Zisman plot			Fowkes			OWK			vOCG				Wu		
	Water	Formamide	Diiodomethane	$\gamma_c$	$\gamma_s^D$	$\gamma_s^T$	$\gamma_s^D$	$\gamma_s^{SP}$	$\gamma_s^T$	$\gamma_s^{LW}$	$\gamma_s^{AB}$	$\gamma_s^+$	$\gamma_s^-$	$\gamma_s^T$	$\gamma_s^D$	$\gamma_s^{SP}$			
CTF	23 $\pm$ 1.1	14 $\pm$ 0.7	31 $\pm$ 1.5	49.2	43.8	57.0	43.8	13.2	56.1	43.8	12.3	0.8	47.0	57.5	44.0	13.5			
TF	24 $\pm$ 1.2	8 $\pm$ 0.4	30 $\pm$ 1.5	56.1	44.2	58.0	44.2	13.8	56.9	44.2	12.7	0.9	44.5	58.5	44.4	14.1			

The  $\gamma_c$  values for both samples were also determined using the Zisman plot method. It can be seen that the CTF had a lower  $\gamma_c$  indicating a more hydrophobic character.

#### 4.4. Mechanical properties of ABS composites

The mechanical properties of ABS composites are displayed in Fig. 4. As a comparison, the neat ABS was also included. It can be observed that the tensile strength of the specimens decreased almost linearly when TF and CTF were incorporated into the ABS matrix. As compared with that for neat ABS (43.8 MPa), the tensile strength decreased from 43.7 to 28.7 MPa and from 42.9 to 29.8 MPa for ABS/TF and ABS/CTF composites, respectively, with the filler loading increasing from 2 to 40 wt%. The tensile strength is more dependent on the filler-matrix interaction. This poor adhesion created weak interface regions, resulting in debonding and frictional pullout. The decrease in the polymer matrix content in the composite as a function of the increase in the filler content was also responsible for the low tensile strength. For tensile modulus, an increasing trend was displayed with the incorporation of TF and CTF in Fig. 4. As compared with that for neat ABS (2307.0 MPa), this value increased by 101 and 52% for TF and CTF, respectively, with the filler loading increasing from 2 to 40 wt%. The apparent increase in Young's modulus was attributed to the increased filler-matrix interfaces and the enhanced load transmission from the polymer

matrix to the reinforcement. The elongation at break in tensile strength of ABS composites displayed a decreasing trend as the filler loading increased. This was because the composites became stiffer with an increasing amount of fillers. As compared with that for neat ABS (13.8%), this value decreased from 24.7 to 2.2% for TF and from 13.3 to 2.1% for CTF, when the filler incorporation increased from 2 to 40 wt%. This decrement was ascribed to the low elongation of filler that restricted the flow of polymer molecules past one another. Similar to the trend recorded for tensile strength, there was an overall decrease in flexural strength for ABS composites filled with TF and CTF. It decreased from 83.6 (for neat ABS) to 60.1 and 60.6 MPa for TF and CTF, respectively, with a filler content of 40 wt%. This behavior was different from the relationship between strength and filler content, as can be expected according to the 'rule of mixtures' models [48]. The apparent decrement could be due to filler defects, which caused crack initiation, filler/matrix debonding and early failure before the load was fully transferred from matrix to filler, and flexural strength decreased accordingly. In contrast to flexural strength, the flexural modulus of the composites increased with an increase in filler content. The modulus increased by 63.3 and 58.2% for TF and CTF, respectively, when the filler amount was increased to 40 wt%. These increments could be attributed to the enhanced stiffness of the composite. For the ABS composites filled with TF and CTF, impact strength showed a significant decreasing trend with an increase in filler content. The

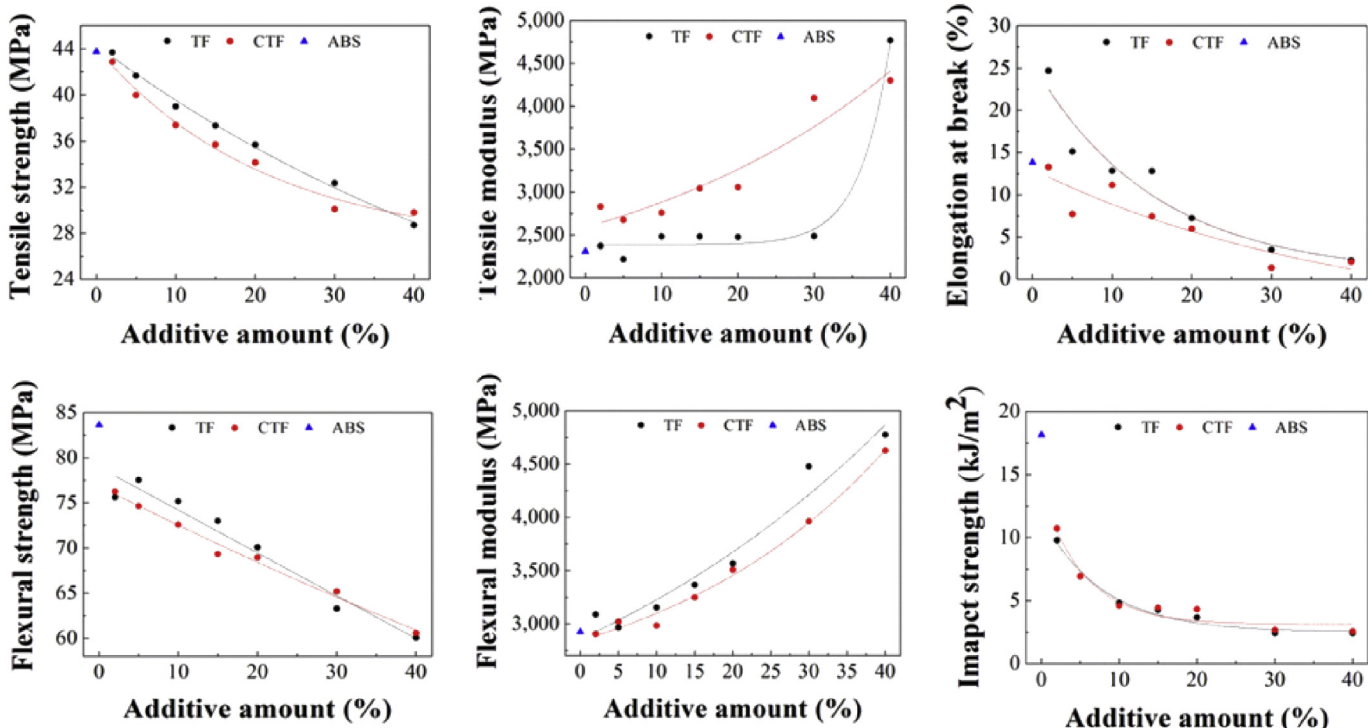


Fig. 4. Mechanical properties of neat ABS and ABS filled with CTF.

presence of filler in the ABS matrix creates points of stress concentration, thus providing sites for crack initiation. Another reason for the decrement in impact strength might be the stiffening of polymer chains due to bonding between filler and matrix. The mechanical properties study showed that incorporation of TF and CTF could increase the tensile modulus and flexural modulus of the ABS matrix, but it decreased the tensile strength, flexural strength, elongation at break and impact strength. Therefore, the inclusion of TF and CTF mainly played a reinforcing role.

## 5. Conclusion

The CTF was prepared and its surface properties were studied and compared to those of TF, using IGC and contact angle measurement. The results showed that the  $\gamma_S^D$  component for both samples contributed the major part of  $\gamma_S^T$ . The values determined using the contact angle methods were consistent, although less than those obtained by IGC analysis. The deconvolution of surface energetic sites confirmed that energetically heterogeneous CTF and TF had variations of surface sites. Compared to  $\gamma_S^D$ , the  $\gamma_S^{SP}$  component contributed less to  $\gamma_S^T$ , implying a lower polarity for both samples. The  $\gamma_S^{SP}$  values calculated by the contact angle methods were consistent, and also lower than those calculated using IGC. The CTF had lower, indicating a more hydrophobic character. The lower  $\gamma_S^D$  and  $\gamma_S^{SP}$  for CTF added up to a lower  $\gamma_S^T$  value, which could reduce filler particle-particle interactions, and thus lead to an increase in ABS/CTF composite performance.

The mechanical properties analysis showed that the inclusion of TF and CTF played mainly a reinforcing role in the filled ABS, and a better mechanical performance for CTF was confirmed. The absence of toxic metals, coupled with suitable mechanical performance, makes CTF a candidate filler for the masterbatch industry.

## Acknowledgments

The authors gratefully acknowledge financial support from the National Natural Science Foundation of China (Grant no. 41373121 and 41101213) and Zhejiang Provincial Natural Science Foundation of China (Grant no. LY14D010009).

## References

- [1] M.B. Bakar, Y.W. Leong, A. Ariffin, Z.A. Ishak, Mechanical, flow, and morphological properties of talc-and kaolin-filled polypropylene hybrid composites, *J. Appl. Polym. Sci.* 104 (2007) 434–441.
- [2] A. Shakoor, N.L. Thomas, Talc as a nucleating agent and reinforcing filler in poly (lactic acid) composites, *Polym. Eng. Sci.* 54 (2014) 64–70.
- [3] H.E. Wiebking, The performance of ultrafine talc in rigid PVC, *J. Vinyl Addit. Technol.* 2 (1996) 187–189.
- [4] Y.T. Sung, P.D. Fasulo, W.R. Rodgers, Y.T. Yoo, Y. Yoo, D.R. Paul, Properties of polycarbonate/acrylonitrile-butadiene-styrene/talc composites, *J. Appl. Polym. Sci.* 124 (2012) 1020–1030.
- [5] W. Qiu, K. Mai, H. Zeng, Effect of silane-grafted polypropylene on the mechanical properties and crystallization behavior of talc/polypropylene composites, *J. Appl. Polym. Sci.* 77 (2000) 2974–2977.
- [6] W. Zhang, A.I. Leonov, IGC study of filler–filler and filler–rubber interactions in silica-filled compounds, *J. Appl. Polym. Sci.* 81 (2001) 2517–2530.
- [7] Y. Wang, W. Lee, Interfacial interactions in calcium carbonate–polypropylene composites. 2: effect of compounding on the dispersion and the impact properties of surface-modified composites, *Polym. Compos.* 25 (2004) 451–460.
- [8] F.M. Fowkes, Determination of interfacial tensions, contact angles, and dispersion forces in surfaces by assuming additivity of intermolecular interactions in surfaces, *J. Phys. Chem.* 66 (1962), 382–382.
- [9] F.M. Fowkes, Chemistry and Physics of Interfaces, Amer. Chem. Soc., Washington, D. C., 1965, p. 1.
- [10] F.M. Fowkes, Additivity of intermolecular forces at interfaces. I. determination of the contribution to surface and interfacial tensions of dispersion forces in various liquids, *J. Phys. Chem.* 67 (1963) 2538–2541.
- [11] G.M. Dorris, D.G. Gray, Adsorption of n-alkanes at zero surface coverage on cellulose paper and wood fibers, *J. Colloid Interface Sci.* 77 (1980) 353–362.
- [12] C.J. Van Oss, R.J. Good, M.K. Chaudhury, Additive and nonadditive surface tension components and the interpretation of contact angles, *Langmuir* 4 (1988) 884–891.
- [13] C.D. Volpe, S. Siboni, Some reflections on acid–base solid surface free energy theories, *J. Colloid Interface Sci.* 195 (1997) 121–136.
- [14] R.R. Smith, D.R. Williams, D.J. Burnett, J.Y. Heng, A new method to determine dispersive surface energy site distributions by inverse gas chromatography, *Langmuir* 30 (2014) 8029–8035.
- [15] A.E. Jefferson, D.R. Williams, J.Y. Heng, Computing the surface energy distributions of heterogeneous crystalline powders, *J. Adhes. Sci. Technol.* 25 (2011) 339–355.
- [16] H.W. Fox, W.A. Zisman, The spreading of liquids on low-energy surfaces. II. Modified tetrafluoroethylene polymers, *J. Colloid Sci.* 7 (1952) 109–121.
- [17] H.W. Fox, W.A. Zisman, The spreading of liquids on low-energy surfaces. III. Hydrocarbon surfaces, *J. Colloid Sci.* 7 (1952) 428–442.
- [18] H.W. Fox, W.A. Zisman, The spreading of liquids on low energy surfaces. I. polytetrafluoroethylene, *J. Colloid Sci.* 5 (1950) 514–531.
- [19] F.M. Fowkes, Determination of interfacial tensions, contact angles, and dispersion forces in surfaces by assuming additivity of intermolecular interactions in surfaces, *J. Phys. Chem.* 66 (1962), 382–382.
- [20] F.M. Fowkes, Attractive forces at interfaces, *Ind. Eng. Chem.* 56 (1964) 40–52.
- [21] D.K. Owens, R.C. Wendt, Estimation of the surface free energy of polymers, *J. Appl. Polym. Sci.* 13 (1969) 1741–1747.
- [22] D.H. Kaelble, Dispersion-polar surface tension properties of organic solids, *J. Adhes.* 2 (1970) 66–81.
- [23] C.J. Van Oss, R.J. Good, M.K. Chaudhury, Additive and nonadditive surface tension components and the interpretation of contact angles, *Langmuir* 4 (1988) 884–891.
- [24] S. Wu, *Polymer Interface and Adhesion*, Marcel Dekker Inc, New York, 1982, pp. 257–259.
- [25] S. Wu, Calculation of interfacial tension in polymer systems, *J. Polym. Sci. Part C Polym. Symposia* 34 (1971) 19–30.
- [26] T. Young, An essay on the cohesion of fluids, in: *Philosophical Transactions of the Royal Society of London*, 1805, pp. 65–87.
- [27] D. Berthelot, Sur le mélange des gaz, *Compt. Rendus* 126 (1898) 1703–1706.
- [28] C.J. Van Oss, M.K. Chaudhury, R.J. Good, Monopolar surfaces, *Adv. Colloid Interface Sci.* 28 (1987) 35–64.
- [29] C.J. Van Oss, R.J. Good, M.K. Chaudhury, Additive and nonadditive surface tension components and the interpretation of contact angles, *Langmuir* 4 (1988) 884–891.
- [30] C.J. Van Oss, M.K. Chaudhury, R.J. Good, Interfacial Lifshitz-van der Waals and polar interactions in macroscopic systems, *Chem. Rev.* 88 (1988) 927–941.
- [31] M. Comard, R. Calvet, H. Balard, J.A. Dodds, Influence of the geological history, particle size and carbonate content on the surface properties of talc as determined by inverse gas chromatography at infinite dilution, *Colloids Surf. A Physicochem. Eng. Aspects* 238 (2004) 37–42.
- [32] M. Comard, R. Calvet, H. Balard, Inverse gas chromatographic study of the surface properties of talc impregnated with different acidic and basic polymers, *Powder Technol.* 128 (2002) 262–267.
- [33] J. Douillard, F. Salles, M. Henry, H. Malandrini, F. Clauss, Surface energy of talc and chlorite: comparison between electronegativity calculation and immersion results, *J. Colloid Interface Sci.* 305 (2007) 352–360.
- [34] G.B. Kaggwa, L. Huynh, J. Ralston, K. Bremmell, The influence of polymer structure and morphology on talc wettability, *Langmuir* 22 (2006) 3221–3227.
- [35] R.F. Giese, P.M. Costanzo, C.J. Van Oss, The surface free energies of talc and pyrophyllite, *Phys. Chem. Min.* 17 (1991) 611–616.
- [36] W. Wu, R.F. Giese, C.J. Van Oss, Change in surface properties of solids caused by grinding, *Powder Technol.* 89 (1996) 129–132.
- [37] J.M. Douillard, J. Zajac, H. Malandrini, F. Clauss, Contact angle and film pressure: study of a talc surface, *J. Colloid Interface Sci.* 255 (2002) 341–351.
- [38] M.D. Ticehurst, R.C. Rowe, P. York, Determination of the surface properties of two batches of salbutamol sulphate by inverse gas chromatography, *Int. J. Pharm.* 111 (1994) 241–249.
- [39] Y. Matsushita, S. Wada, K. Fukushima, S. Yasuda, Surface characteristics of phenol-formaldehyde-lignin resin determined by contact angle measurement and inverse gas chromatography, *Ind. Crops Prod.* 23 (2006) 115–121.
- [40] J.W. Dove, G. Buckton, C. Doherty, A comparison of two contact angle measurement methods and inverse gas chromatography to assess the surface energies of theophylline and caffeine, *Int. J. Pharm.* 138 (1996) 199–206.
- [41] O. Planinšek, A. Troják, S. Srčić, The dispersive component of the surface free energy of powders assessed using inverse gas chromatography and contact angle measurements, *Int. J. Pharm.* 221 (2001) 211–217.
- [42] N.M. Ahfat, G. Buckton, R. Burrows, M.D. Ticehurst, An exploration of interrelationships between contact angle, inverse phase gas chromatography and triboelectric charging data, *Eur. J. Pharm.* 9 (2000) 271–276.
- [43] S.K. Papadopoulou, G. Dritsas, I. Karapanagiotis, I. Zuburtikidis, C. Panayiotou, Surface characterization of poly (2, 2, 3, 3, 3-pentafluoropropyl methacrylate) by inverse gas chromatography and contact angle measurements, *Eur. Polym. J.* 46 (2010) 202–208.
- [44] H.E. Newell, G. Buckton, Inverse gas chromatography: investigating whether the technique preferentially probes high energy sites for mixtures of crystalline and amorphous lactose, *Pharm. Res.* 21 (2004) 1440–1444.
- [45] W. Shen, Y.J. Sheng, I.H. Parker, Comparison of the surface energetics data of eucalypt fibers and some polymers obtained by contact angle and inverse gas chromatography methods, *J. Adhes. Sci. Technol.* 13 (1999) 887–901.

- [46] P.N. Jacob, J.C. Berg, Acid-base surface energy characterization of microcrystalline cellulose and two wood pulp fiber types using inverse gas chromatography, *Langmuir* 10 (1994) 3086–3093.
- [47] J.M. Felix, P. Gatenholm, Characterization of cellulose fibers using inverse gas chromatography, *Nordic Pulp Pap. Res. J. Swed.* 8 (1993) 200–203.
- [48] G. Kalaprasad, K. Joseph, S. Thomas, C. Pavithran, Theoretical modelling of tensile properties of short sisal fibre-reinforced low-density polyethylene composites, *J. Mater. Sci.* 32 (1997) 4261–4267.